PCCP

PAPER

View Article Online
View Journal | View Issue

Cite this: *Phys. Chem. Chem. Phys.*, 2014, **16**, 4386

Micro- or nanorod and nanosphere structures derived from a series of phenyl-porphyrins†

M. Harsha Vardhan Reddy,[a] Rusul M. Al-Shammari,[a] Nebras Al-Attar,[a] Eamonn Kennedy,[a] Luke Rogers,[b] Sergio Lopez,[c] Mathias O. Senge,[b] Tia E. Keyes[c] and James H. Rice*[a]

Received 22nd November 2013,
Accepted 6th January 2014

DOI: 10.1039/c3cp54936d

www.rsc.org/pccp

We examine here a series of *meso*-phenyl porphyrin micro- and nanostructures. Optical absorption and emission spectroscopy imaging and atomic force microscopy are used to investigate the effect of peripheral groups in nano- and microstructures of 5,10,15,20-tetraphenylporphyrin (H_2TPP) compared to three other phenylporphyrins, *i.e.* 5,10,15-triphenylporphyrin (H_2-Tri-PP), 5,10-diphenylporphyrin ($H_2$5,10-BPP) and 5,15-diphenylporphyrin ($H_2$5,15-BPP) molecules. We show that nanospheres and nanorods are formed, the occurrence and properties of which are influenced by the number and position of the phenyl substituents.

1. Introduction

A considerable amount of research has been undertaken to advance the understanding of optical processes in low dimensional nanomaterials such as quantum dots, nanodisks, fullerenes and carbon nanotubes.[1–10] Self-assembled nano- and micro-structured aggregates of π-conjugated molecules are of interest due to their structural similarities to photosynthetic antenna systems of green bacteria.[11–13] Such antenna systems channel the energy to the photosynthetic reaction center where light is converted into chemical energy *via* a charge separation process. It is believed that the complex self-assembling antenna systems are the reason for the extraordinary light collection efficiency in photosynthesis.[14] In the chlorosomes of green bacteria, bacterio-chlorophylls (a porphyrin derivative) assemble to form nanorods, and these chromosomal rods are the most efficient harvesters of light known.[15] This has motivated research into understanding the processes and structure of porphyrin nano(rod) materials.

Synthetic porphyrin nanorods offer the potential to mimic naturally occurring nanorods (*e.g.* chromosomal rods). The use of synthetic materials offers potential advantages over the use of biological materials such as in the cost of production and scalability of production. The ability to alter the chemical structure (*via* synthetic chemical methods) to optimise the nanorod material for the application in question is also an advantage. One way to produce efficiently porphyrin nanorods is *via* self-assembly. Self-assembly occurs whereby molecules, atoms or nanoparticles spontaneously form pre-designed structures, typically through non-covalent interactions such as π–π stacking, hydrophobic–hydrophobic interactions H-bonding, electrostatics, *etc.*[16–20]

Nano- and micro-structured porphyrin aggregates can self-assemble to form highly stabile nano- and micro-rod or wire like structures. The synthetic porphyrin $TPPS_4$ is a widely studied porphyrin that forms spontaneously nanorod structures in highly acidic aqueous solutions.[21] In neutral and basic solutions electrostatic repulsion prevents $TPPS_4$ aggregation, with increasing acidity two protons bind to the inner pyrrole nitrogen atoms forming the porphyrin diacid. The presence of these two protons induces a strong, saddle-type distortion of the porphyrin ring, further decrease of pH results in two additional protons being bound to two of the sulfonate groups, forming a zwitterionic species that self-assembles into micro- and nanorod-like aggregates, stabilized by Coulombic and π–π interactions. A range of porphyrins have been found to form nanorod like structures. One approach applies ionic self-assembly of two oppositely charged porphyrins in aqueous solution such as $TPyP^+$ and $TSSP^-$.[21,22] Nanorods of metal-free H_2TClPP made using nanoporous anodized aluminum oxide membranes have been reported.[23] ZnTPyP has been reported to form nanorod-like structures made *via* aggregation using surfactant-assisted cooperative interactions.[24]

An alternative approach to the formation of micro- and nanostructures such as nanorods or nanowires based on porphyrin aggregates is to use water insoluble porphyrins such as H_2TPP which is a stable synthetic porphyrin. However, studies on aggregation behaviour of water-insoluble porphyrins are limited. Okada and Segawa[25] reported that the water-insoluble porphyrin H_2TPP forms J-aggregates in acidic solution. Other water insoluble porphyrin aggregates that have been studied include ZnTPP which was reported to exist as J-aggregates in high polarity

[a] *NanoPhotonics Research Group, University College Dublin, Dublin, Ireland. E-mail: james.rice@ucd.ie*
[b] *School of Chemistry, Trinity College Dublin, Dublin, Ireland*
[c] *School of Chemical Science, Dublin City University, Dublin, Ireland*

† Electronic supplementary information (ESI) available. See DOI: 10.1039/c3cp54936d

solvent creating nanowire structures.[26] Octaethyl porphyrin also forms J aggregates that form nanowires.[27]

Introduction of substituents at the *meso* position can significantly modulate the electronic properties of porphyrins.[28–31] Additionally, peripheral substitution often brings about the distortion of the porphyrin ring system *via* out-of-plane and in-plane distortion which is crucial for their biological function.[29–33] In this context, a series of porphyrins with the same substituent but different substituent numbers are useful compounds to study the structure–property relationship of porphyrins.[32,33–35] Particularly a partial substitution at the *meso* positions, *i.e.* the so-called A_x-porphyrins,[36,37] was found to bring about remarkable in-plane distortion and may be used as an ideal model to study the effects of in-plane distortion on porphyrin properties.[30–33,36–40] Various forms of aggregates (*e.g.*, face-to-face dimers, H- and J-aggregates) have been inferred in interpreting optical absorption spectral changes and variations in the fluorescence quantum yields of porphyrins.[41–43] Studies have shown that several factors influence the extent of aggregation in porphyrin systems, notably the number and nature of peripheral groups in the porphyrin molecule or pH of the environment. Porphyrins can form J- or H-type aggregates. J-aggregates occur when the transition dipole moments of the porphyrins are aligned parallel (''head-to-tail''). In H-aggregates, the transition dipole moments of the monomer molecules are perpendicular to the line of centres (''face-to-face''). Porphyrin aggregates can form specific structures dependent upon pH. For example, some porphyrins can form rod like structures.[20–27,44] It is noted that the ability of porphyrins to form such structures depends on factors such as the side group number and type.

We examine here the influence of the porphyrin phenyl substituent position and the number of phenyl substituents on the formation of porphyrin micro- and nanostructures. We study the effect of different numbers of phenyl groups on aggregation in *meso*-tetraphenyl porphyrins in order to assess the role that such groups have on this process. Optical absorption and emission spectroscopy along with fluorescence (lifetime) imaging and atomic force microscopy are used to investigate the effect of peripheral groups in J-aggregates of 5,10,15,20-tetraphenylporphyrin (H_2TPP) compared to three other phenylporphyrins, *i.e.* 5,10,15-triphenylporphyrin (H_2TriPP), 5,10-diphenylporphyrin (H_2-5,10-BPP) and 5,15-diphenylporphyrin (H_2-5,15-BPP) molecules. We show that nanospheres and micro/nanorods are present, the occurrence of which are influenced by the number and position of the phenyl substituents.

2. Experimental

The phenylporphyrins were synthesized as reported earlier.[36] The phenyl-porphyrin samples were made by drop deposition of the porphyrins onto a glass slide using dichloromethane as the carrier solvent. The porphyrins were prepared as thin films. Two sets of samples were prepared. The first set of samples were prepared by deposition of porphyrins directly onto a glass slide under neutral conditions. The second set of samples were prepared by depositing the porphyrins onto a slide in the presence of acid. The acid solution used was H_2SO_4 acid pH = 0.1. In all cases the samples were dried in air. All solvents were purchased from Sigma-Aldrich (as analytical grade solvents were applicable) and used as received. Optical UV/vis absorption spectra were recorded using a Bruker UV/Vis instrument. The samples were prepared as thin films by drop deposition onto a glass slide. Atomic force microscopy (AFM) studies were performed using an Explorer AFM. Fluorescence microscopy studies were performed using a Zeiss inverted microscope system coupled with a 532 nm excitation wavelength, a CCD camera and a 650 nm band pass filter. The resulting images were fitted with scale bars that indicate length. A Picoquant Microtime 200 fluorescence lifetime imaging microscopy (FLIM) system was used for lifetime imaging.

3. Results and discussion

Absorption spectra of two H_2TPP porphyrin films, one prepared as a neutral film (in the absence of acid for comparison) and a film prepared with acid (pH = 0.5), are shown in Fig. 1a. The neutral porphyrin film shows an absorption spectrum that has an intense Soret (or B) band and four weak Q bands (Q_1 to Q_4, band positions outlined in Table 1).

These absorption bands are understood to arise from transitions between two HOMOs and two LUMOs in the porphyrin where the HOMO and HOMO − 1 are nearly degenerate and the LUMO and LUMO − 1 are degenerate.[40] The mixing of these bands creates a higher energy 1 e_u state with greater oscillator strength, giving rise to the Soret band, and a lower energy 1 e_u state with less oscillator strength, giving rise to the Q-bands. Following the addition of acid the absorption spectrum for H_2TPP shows different spectral features compared to when acid is absent (see Table 1). A large band (marked A_2 *i.e.* a band at 716 nm) is seen in the acidic film which is absent in the neutral H_2TPP film. In the Soret band region two bands are observed

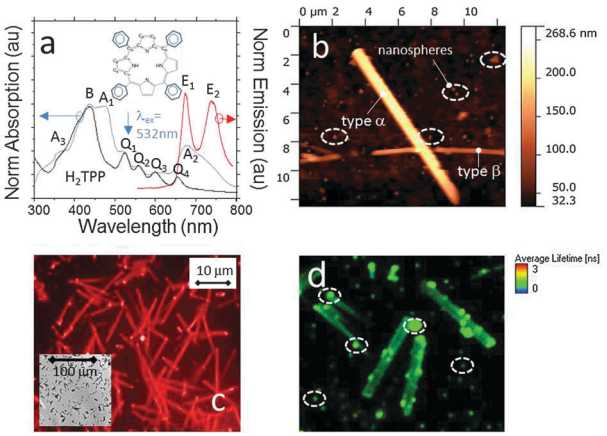

Fig. 1 Studies of J-H2TPP. (a) Optical absorption and emission spectra, the inset shows a schematic drawing of the molecule. (b) AFM topography image, circled are nanospheres. (c) Fluorescence microscopy image, inset: optical transmission image. (d) FLIM image, circled are examples of where nanosphere like structures occur.

Table 1 Band positions from optical absorption spectra of all four porphyrins

		Absorption							
		Band positions (nm)							
					Q bands				
Porphyrin	pH	A_3*	Soret B	A_1*	Q_1 $Q_{y(0-1)}$	Q_2 $Q_{y(0-0)}$	Q_3 $Q_{x(0-1)}$	Q_4 $Q_{x(0-1)}$	A_2
H_2TPP	Neutral		435		522	566	596	652	
	0.5	365	436	473	519	555	598	678	716
H_2Tri-PP	Neutral		430		518	550	590	645	
	0.5	365	430	460	518	550	590	545	665
$H_2$5,15 Di-PP	Neutral		417		516	546	587	638	
	0.5	365	418	460	515	546	587	635	
$H_2$5,10 Di-PP	Neutral		414		506	541	582	635	
	0.5		413		506	558	582	634	

(marked B and A_1 *i.e.* bands at 436 and 473 nm, respectively) in the acidic film while in neutral H_2TPP only one band is present in this region *i.e.* the B band. A small band marked A_3 (at 365 nm) can be seen in the acidic film that does not appear in neutral H_2TPP.

Porphyrins can form J or H-type aggregates where the ability of porphyrins to form such structures depends on factors such as the side group number and type.[41–44] The optical absorption spectrum for H_2TPP at pH = 0.5 (Fig. 1a) shows the occurrence of 'red-shifted' bands relative to B and Q bands, these are marked A_1 and A_2. These 'red-shifted' bands are characteristic of J-aggregates.[41–44] 'Blue-shifted' bands *e.g.* A_3 are characteristic of H-aggregates. Thus the absorption spectrum indicates that H_2TPP forms J-aggregates, with some indication that H-aggregates also form simultaneously. On the basis of the relatively large absorption bands assigned to J-aggregates compared to the relatively small H-aggregate band (not withstanding absorption cross section differences), the sample is assigned to be predominantly J-aggregate.

The J-aggregate H_2TPP porphyrin film (J-H_2TPP) was studied using AFM. AFM imaging was applied to determine information in regard to the size and the shape of the structures formed. Fig. 1b shows an AFM image of the J-H_2TPP sample (see also Fig. S6, ESI†). A number of nanostructures can be seen in the image that possesses a rod like structure. Table 2 outlines a set of average feature sizes. The geometric structure of the nanostructures on average come in two different sizes, a large nanorod like structure (type α) with an average feature size of 10.7 micron length, 1.4 micron diameter and 250 nm height *i.e.* a micro-rod like structure. A second type (type β) possessing average features of 4.1 micron length, 758 nm diameter and 119 nm height. Although lengths are comparable the aspect ratio of these rods is very different. From AFM analysis micro- and nanosized rods are seen dispersed on the substrate. It is noted that the size of the nanorods for H_2TPP porphyrin are much larger than the reported feature sizes of the nanorods made from H_2TSPP aggregates, which form nanorods about 3.8 nm in diameter on mica, graphite, and polystyrene.[12]

Inspection of the AFM topography image in Fig. 1b shows also the presence of sphere like structures. The size of the spheres was on average 150 nm in diameter *i.e.* they are nanosized spheres (nanospheres). Nanospheres are marked with circles for clarity in Fig. 1b. These nanospheres are present on the substrate surface and also on the nanorods occurring in large numbers across the sample.

Studies of the micro- and nanorod samples were made using optical transmission contrast imaging and fluorescence microscopy (Fig. 1c and see ESI,† Fig. S1). Optical transmission imaging shows rod-like structures of various lengths and widths. These structures are found in large numbers across the substrate. Fig. 1c and ESI† Fig. S1 show fluorescence microscopy and optical transmission images of the substrate. Fluorescence microscopy images show in red micro- and nanorod and nanosphere shapes occurring at relatively high concentrations on the substrate. The J-H_2TPP micro- and nanorods emit strongly when excited at 532 nm, which is in resonance with the Q band absorption region for the porphyrin. The emission spectrum from J-H_2TPP is shown in Fig. 1a. The J-H_2TPP nanorods emit at *ca.* 663 and 730 nm. The emission is assigned to fluorescence. The fluorescence spectrum shows the appearance of two peaks. These two broad bands are assigned to arise from the Q(0,0) and Q(0,1) bands, respectively. These broad bands can be de-convoluted into four different sub-bands.[26] These four bands can be

Table 2 Feature sizes derived from AFM topography imaging for all four porphyrins. The data were compiled from 30 image scans of each sample

Porphyrin		Diameter (nm)	Height (nm)	FWHM (nm)	Length (nm)
H_2TPP	Type α	1380 (sd = 294)	250 (sd = 73)	954 (sd = 73)	10.7 (sd = 0.79)
	Type β	758 (sd = 193)	119 (sd = 39)	489 (sd = 136)	4.1 (sd = 1.5)
H_2Tri-PP		838 (sd = 192)	96 (sd = 31)	58b (sd = 188)	15.32 (sd = 3.87)
$H_2$5,15 Di-PP		3067 (sd = 302)	1055 (sd = 125)	2144 (sd = 324)	27.5 (sd = 0.162)

assigned to arise from the monomer and from the aggregate (two bands each from the monomer or aggregate).

The optical properties of the J-H_2TPP rod samples were further probed using fluorescence lifetime imaging (FLIM). This technique gives an additional support to the elucidation of shapes accepting that the image resolution is diffraction-limited.[45–47] The FLIM images are collected at ~300 nm spatial resolution and with ~500 picosecond temporal resolution. Fig. 1d shows FLIM images for J-H_2TPP nanorods. The FLIM images show a large concentration of rods dispersed across the sample. Fluorescence lifetimes from the rods are <3 ns upon inspection. The FILM image shows approximate uniform lifetimes across the sample indicating a large degree of homogeneity in the material. This suggests that the self-organised nanorods involve a single form of porphyrin aggregate *i.e.* as J-aggregates. The lifetime of the fluorescence is similar across the sample resulting in a homogeneous lifetime (as was measured with an error of ±500 ps). The FLIM image shows the presence of rods and spheres, with the sphere shapes (nanospheres) emitting at a similar intensity to the rods. These nanospheres showing a fluorescence lifetime (within an error of ±500 ps see below) as the rods as the FLIM colour map shows. Nanospheres are marked with circles for clarity.

Fig. S2 (ESI†) shows the lifetime of several rods and nanospheres taken from FLIM images, the average lifetime = 1.73 ns ± 0.5 ns. Analysis of the exciton recombination lifetime of a single nanosphere (see Fig. S2, ESI†) and a single rod (see Fig. S2, ESI† also) yields lifetimes of 1.32 ns ± 0.5 ns and 1.66 ns ± 0.5 ns, respectively. The lifetimes obtained for the single rod and nanosphere were within a 0.5 ns difference as was the average lifetime for a collection of rods and nanospheres. On this basis we assert that the exciton recombination lifetime is assigned to be the same for nanospheres as for rod structures.

Studies of H_2-Tri-PP were undertaken. The effect of adding acid to H_2-Tri-PP was studied using absorption spectroscopy. Fig. 2a shows the absorption spectrum for H_2-Tri-PP with and without the addition of acid. The addition of acid creates a change in the absorption spectral features with bands at A_1, A_2 and A_3 formed. The band positions for the absorption spectra are outlined in Table 1. The spectral features are similar to those seen for H_2TPP with strong bands at A_1 to A_3 formed with acid. On this basis we assign the acid H_2-Tri-PP film structure to come from J-aggregates (hereafter referred to as the J-H_2-Tri-PP film).

The J-H_2-Tri-PP film was studied using AFM. AFM topography imaging shows that nanorods are formed on the substrate. The formation of sphere shaped nanostructures is also observed on the substrate. Fig. 2b shows an AFM scan of J-H_2-Tri-PP. The image shows the presence of rods and also spheres. Spheres are marked with circles for clarity in the image. The spheres occur over the sample in large numbers. AFM showed that on average the nanorods were 15 microns long with a diameter of 838 nm and a height of 96 nm. Table 2 outlines average structural properties as found from inspection of over 30 nanorods taken from AFM topography images. This confirms that the transmission contrast images show rod-like structures as for H_2TPP (see Fig. 2c and ESI,† Fig. S3). The spheres are on average 150 nm in diameter (*i.e.* nanospheres).

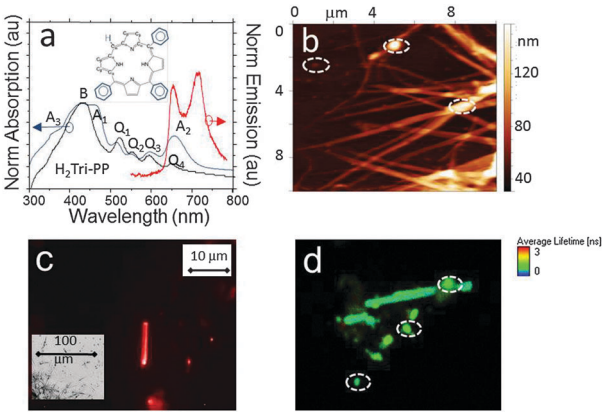

Fig. 2 Studies of the H_2-Tri-PP aggregate sample. (a) Optical absorption and emission spectra, the inset shows a schematic drawing of the molecule. (b) AFM topography images, circled are nanospheres. (c) Fluorescence microscopy image, inset: optical transmission image. (d) FLIM image, circled are nanospheres.

Studies of the J-H_2-Tri-PP nanorod samples were made using optical transmission contrast imaging (Fig. 1c inset and see ESI,† Fig. S3) and fluorescence microscopy. The micro- and nanorods and nanospheres are fluorescent. Fig. 1c shows a fluorescence microscopy image of the substrate. In red are rod and nanosphere shapes occurring at relatively high concentrations on the substrate. Polarisation fluorescence measurements showed that polarisation of the emission was present. J-H_2-Tri-PP rod samples were probed using fluorescence lifetime imaging (FLIM). Fig. 2c shows FLIM images for J-H_2-Tri-PP rods. The FLIM image shows the presence of rods and spheres, with the sphere shapes (nanospheres) emitting with *ca.* the fluorescence lifetime as the rods as the FLIM colour map shows. The average lifetimes from the rods and nanospheres are 1.9 ns ± 0.5 ns. Not enough signal intensity was available in the images recorded to assess the lifetimes for single nanospheres or single rods alone. The FILM image shows approximate uniform lifetimes across the sample indicating a large degree of homogeneity in the material. This in turn indicates that the organisation of the porphyrins *i.e.* as J-aggregates is similar across the sample resulting in a homogeneous lifetime.

Studies of $H_2$5,15 Di-PP were undertaken as shown in Fig. 3. The effect of adding acid to $H_2$5,15 Di-PP was studied using absorption spectroscopy. Comparing the absorption spectra with and without acid shows the presence of strong A_1 and A_3 bands indicating that aggregation has occurred (Fig. 3a). However the absence of a strong A_2 band suggests that the degree of J-aggregation is reduced. A strong A_3 band is seen suggesting that H-aggregation is present and may be occurring to a greater degree than for H_2TPP and H_2-Tri-PP. On this basis we refer to the aggregated film as H/J-$H_2$5,15 Di-PP. The H/J-$H_2$5,15 Di-PP film was studied using AFM. AFM topography imaging shows that rods are formed. The rods that are formed are present in a reduced concentration than for the previous two porphyrins *i.e.* the concentration of the nanostructures being approx. a magnitude less in concentration. (H_2TPP and H_2-Tri-PP). Sphere shaped nanostructures are also observed on the substrate.

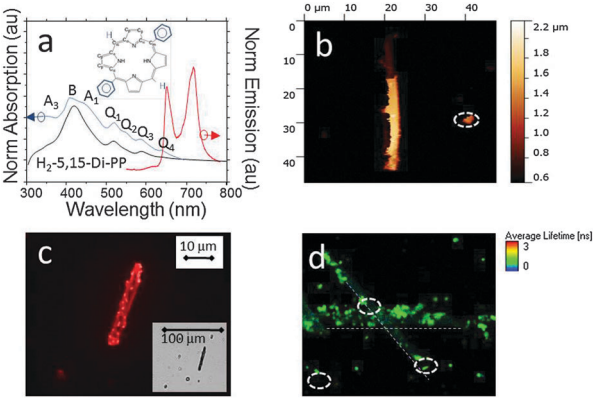

Fig. 3 Studies of the $H_2$5,15 Di-PP aggregate sample. (a) Optical absorption and emission spectra, the inset shows a schematic drawing of the molecule. (b) AFM topography images, circled are nanospheres. (c) Fluorescence microscopy image, inset: optical transmission image. (d) FLIM image, circled are nanospheres, dashed-lines are present to guide the eye in regard to the presence of micro-rods.

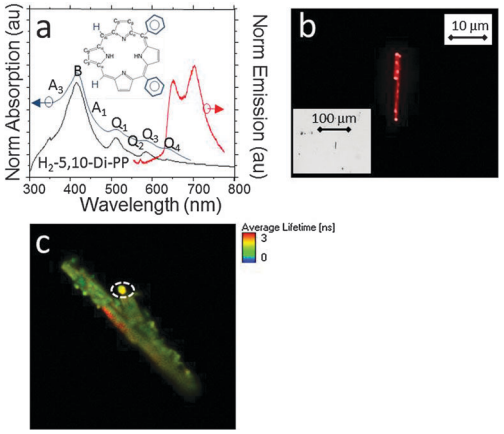

Fig. 4 Studies of $H_2$5,10 Di-PP aggregates. (a) Optical absorption and emission spectra, the inset shows a schematic drawing of the molecule. (b) Fluorescence microscopy image, inset: optical transmission image. (c) FLIM image, circled is a sphere.

Fig. 3b shows an AFM scan. Nanosized spheres are marked with circles for clarity, being *ca.* 500 nm in diameter. From several AFM measurements it was estimated that the size of the rods (see Table 2) was larger than for the previous two porphyrins. The average feature size was 27.5 micron length, 3.1 micron diameter and 1.1 micron height, *i.e.* micro-rod structures.

Studies of the H/J-$H_2$5,15 Di-PP rod samples were made using optical transmission contrast and fluorescence imaging (Fig. 1c and see ESI,† Fig. S4). The images show a large number of rod-like structures of various lengths and widths. The rods (and also nanospheres seen) are fluorescent. H/J-H_2 5,15 Di-PP samples were probed using fluorescence lifetime imaging (FLIM). Fig. 3d shows FLIM images for H/J-$H_2$5,15 Di-PP. The lifetime from the micro-rods is 1.7 ns $\pm$ 0.5 ns for the nanorod shown. The FILM image shows approximate uniform lifetimes across the nanorod indicating a large degree of homogeneity in the material. The FLIM image shows the presence of rods and spheres. A faint, weak emission can be seen from a rod like shape, while strong emission from nanospheres can be seen.

Studies of $H_2$5,10 Di-PP were undertaken as shown in Fig. 4. The effect of adding acid to $H_2$5,10 Di-PP was studied using absorption spectroscopy. Comparing the absorption spectra with and without acid shows minor differences in regard to relative intensities of Q bands to B bands, with a more pronounced Q_4 band (magnified in Fig. 4a for clarity as for $H_2$5,10 Di-PP). This indicates that some aggregation has potentially occurred but to a very small extent compared to the other porphyrin samples studied. The $H_2$5,10 Di-PP film was studied using AFM, however no sign of rods was found. Optical transmission and fluorescence images (see Fig. 4b and ESI,† Fig. S5) indicated that rod like structures were present but at much lower concentrations (too infrequent for AFM studies). The fluorescence microscopy image shows that the rod like structure has a number of spheres superimposed on the structure. This indicates that the rod has only weakly formed (from cohesion of spheres potentially) $H_2$5,10 Di-PP rod samples probed using fluorescence lifetime imaging (FLIM). Fig. 4c shows FLIM images for $H_2$5,10 Di-PP rods. The lifetimes of the nanorods are *ca.* 1.78 ns. This lifetime was the average lifetime. Inspection of the microrod structure in Fig. 4c shows that part of the rods has a different colour *i.e.* red compared to the remaining rods which are green in colour; this indicates that the lifetime of the rods varies. This is the subject of further study.

The UV/vis absorption band positions for all four porphyrins are outlined in Table 1 (and are shown together in ESI,† Fig. S7). Analysis of the band positions for porphyrins without acid shows a redshift of the Soret band and Q bands with increasing phenyl numbers. The Soret band shifts sequentially from 414 to 417 nm for di-phenyl TPP, to 430 nm for tri-phenyl TPP and to 435 nm for tetra-phenyl TPP. This is in line with calculations of the electronic orbital energy levels for the four phenyl porphyrins which show that the HOMO–LUMO red-shifts with increasing phenyl numbers *i.e.* from 2.9104 eV for di-phenyl TPP to 2.6955 eV for tetra-phenyl TPP.[41] Following aggregation J-aggregation occurs (as outlined above). Kasha's analysis of energy relaxation from excited states of molecular aggregates predicts that a stacked face-to-face H-aggregate leads to a spectral blue shift relative to the monomer excited-state level, whereas a tilted "deck of cards" (J-aggregate) aggregation leads to a red shift in the Soret band.[41] Khairutdinov *et al.* noted that the extent of this shift is proportional to the degree of aggregation, the interplanar separation distance, mutual orientation of the monomers in the aggregate, electronic transition probabilities, and the specific sensitivities of the chromophore.[41] It is known that intermolecular electronic interactions within the aggregates cause the degeneracy in the excited-state electronic energy levels to be lifted. For J-aggregates, transitions to the lower energy excited state are allowed, resulting in the red shift of their absorption bands. For porphyrins containing phenyl groups, *e.g.* H_2TPP, an additional red shift of the absorption may occur because of enhanced coplanarity between the porphyrin core and the phenyl rings (enhanced conjugation of phenyl rings to the porphyrin core) within the J-aggregates, a result of

molecular packing constraints.[41] For H_2TPP in an acidic environment (as outlined in Table 1) the optical absorption band features are assigned to arise from the formation of various J-aggregates. Inspection of the magnitude and intensity of the B and Q bands from the absorption spectra for all four tetraphenyl porphyrins show that on the basis of the degree of spectral changes of the aggregate from the neutral porphyrin film, the degree of aggregation ranges from H_2TPP > H_2-Tri-PP > H_2-5,15-BPP > H_2-5,10-BPP. A small blue shift is also noted indicating the presence of H-aggregates. Bands at *ca.* 350 nm could be observed in all four porphyrins (A_3 band). Fig. 3a shows that for H_2-5,15-Di-PP features associated with H-aggregates are more prevalent than for J-aggregates. This shows that the structure of the porphyrin is important in regard to the ability to form J (or H) aggregates. This may be due to the ability of the porphyrin to pack or arrange into structures such as the ''deck of cards'' outlined above.

The optical transmission and fluorescence microscopy images for H_2TPP (see Fig. 1 and ESI,† Fig. S1) show the presence of micro- and nanorods and nanospheres occurring in significant numbers. The images show that the micro/nanorods and nanospheres occur randomly over the substrate. The orientations of the micro/nanorods are random. Examination of the microscopy images indicates that the tips of micro/nanorods possess more fluorescence intensity than the other parts of the rods (see ESI,† Fig. S1). It is noted that this may arise from a nanosphere located on the micro/nanorods at the rod tip giving rise to this effect. An alternative explanation may be that the micro/nanorod waveguides the light to its tips giving rise to this larger emission intensity. Examination of H_2-Tri-PP (see ESI,† Fig. S3) shows that the tips of nanorods possess more fluorescence intensity than the other parts of the rods as for H_2TPP possibly indicating that waveguiding potentially occurs also for this porphyrin nanotube. Nanospheres are also observed to be emitting with an intensity *ca.* the same as the rods. It is noted that while waveguiding may be present another explanation may be that the termini of the structures possess less order (therefore the molecular dipoles are less ordered) and potentially a higher quantum yield may arise from these sites. The occurrence of the micro/nanorods is relatively common over the substrate along with nanospheres. Optical transmission images for $H_2$5,15 Di-PP (see ESI,† Fig. S4) show that large micro-rods are present in low numbers over the substrate, along with relatively large nanospheres. Examination of the micro-rod optical transmission image was undertaken by changing the contrast. At high contrast only the areas around the edges of the micro-rod are visible. This area is seen potentially to be made of nanosized spheres, with decreasing contrast more of the rod is seen obscuring the presence of nanospheres and a more defined rod shape is seen. Examination of the fluorescence image for $H_2$5,15 Di-PP (see ESI,† Fig. S4) shows the presence of large numbers of nanospheres on the nanorod surface, supporting the optical transmission data. One explanation of this is that the micro-rod may form from a large number of nanospheres condensing together to form a crystalline like aggregate rod structure. Optical transmission and fluorescence images for $H_2$5,10 Di-PP (see ESI,† Fig. S5) show a similar effect with nanospheres located over the nanorod structure. In addition the number of micro/nanorods was too low for AFM measurements to find and image.

AFM image analysis (see Table 2) shows that the size of the micro-rod formed increases H_2TPP to H_2-Tri-PP to H_2-5,15-BPP as defined by rod length. This is inversely related to the degree of J-aggregation indicating that more efficient the J-aggregation the better the rod formation. This by extension can include data from water soluble porphyrins which form efficiently J-aggregates (*e.g.* H_2TPPS) and yield rods with smaller dimensions. However, it is noted that the nano/microrod structures may arise from other causes apart from J-aggregates. It is noted that while J-aggregates are characterized by a red shift of their absorption bands as compared to the positions of the monomeric species, there are many possible reasons for a porphyrin-derived material to exhibit red shifted features. Studies by Chernia and Gill[48] found that for H_2TMPyP^{4+} and metallo ZnTMPYP surface effects/interactions can give rise to red-shifts in absorption spectra. Studies by Rosa *et al.*[49] reported that porphyrin-core saddling and twisting of *meso*-aryl substituents can give rise to an absorption red-shift. Stone and Fleischer[50] reported that core protonation creates an absorption red-shift. The formation of microscopic needle-shaped crystals of the TPP diacid derivative and/or a mix of free base and diacid derivatives may be present creating the observed UV/Vis absorption spectral profiles seen in Fig. 1a–4a. TPP diacids exhibit red-shifted bands with respect to the free base, and their films would exhibit broadened extinction bands due to the presence of non-negligible scattering components in the UV-vis spectrum. Polarized fluorescence microscopy studies indicate that the nano/mircorods are crystalline.

Okada and Segawa[25] reported that porphyrin J-aggregates of various water-insoluble tetra-phenylporphyrin derivatives form microcrystalline structures on the basis of the observed red-shift in the absorption spectra. The authors noted that the lower exciton (S_1 *i.e.* A_2 in Table 1) markedly depends on *meso*-substituents, whereas higher exciton (S_2 *i.e.* A_1 in Table 1) does not depend on them. The authors noted that the nature of the exciton coupling of the S_1 transition dipole moment can be systematically changed by the substituents. This is broadly in line with our studies in regard to the position and intensities of the S_1 transition being affected by the numbers of phenyls where when 4 phenyl groups are present a strong S_1 transition is seen which is blue shifted and reduced in relative intensity when 3 phenyl groups are present, while when 2 phenyl groups are present no S_1 transition can be seen. Okada and Segawa[25] noted that the dication absorption (for S_2 or A_1 in Table 1) is at 438 nm while the S_2 band is at 475 nm for the J-aggregate. It is noted that we report a S_2 band at 473 nm. This indicates that the porphyrins in our study arise from J-aggregates not dications.

Studies by Kaupp *et al.*[51] showed that for H2TPP in acid solutions (pH = 0.7 and below) the mono-protonated TPP dimer possesses a Soret band at 465 nm and another mono-protonated TPP dimer with a Soret band at 403 nm is also reported that differs in orientation of dipole transition

moments in the neighbouring molecules. Di-protonated TPP dimers with a Soret band at 415 nm were also reported. The formation of the J-aggregates may be a result of mono-protonated TPP dimer formation; Fig. 1 shows a Soret band at 475 nm, which is close to the reported Soret band position for mono-protonated TPP dimers.

4. Conclusions

In summary, a series of phenyl-porphyrins (5,10,15,20-tetraphenylporphyrin (H_2TPP), 5,10,15-triphenylporphyrin (H_2-Tri-PP), 5,10-diphenylporphyrin ($H_2$5,10-BPP) and 5,15-diphenylporphyrin ($H_2$5,15-BPP)) were demonstrated to form nano- and micro-structures in an acidic environment. Optical absorption and emission spectroscopy showed that mono-protonated TPP dimers are formed, and evidence for the formation of J-aggregates was also found. Optical and AFM imaging showed the presence of rod and sphere like structures. The rod-like structure dimensions were found to be related to the type of porphyrin present, with the size of the rods increasing for H_2TPP < H_2-Tri-PP < $H_2$5,15-BPP.

Acknowledgements

This work was supported by grants from Science Foundation Ireland (SFI P.I. 09/IN.1/B2650) and (10/IN.1/B3025). The Nanophotonics and Nanoscopy Research Group is supported by SFI grants 11/RFP.1/MTR/3151, 12/IP/1556 and 09/RFP/PHY2398.

References

1 J. C. Charlier, *Acc. Chem. Res.*, 2002, **35**, 1063.
2 J. H. Rice, J. W. Robinson, A. Joujour, R. A. Taylor, R. Oliver and G. A. D. Briggs, *Appl. Phys. Lett.*, 2004, **84**, 41101.
3 C. M. Drain, A. Varotto and I. Radivojevic, *Chem. Rev.*, 2009, **109**, 1630–1658.
4 J. H. Rice, J. P. Galaup and S. Leach, *Chem. Phys.*, 2002, **279**, 23.
5 J. H. Rice, J. P. Galaup and S. Leach, *Chem. Phys.*, 2001, **263**, 401.
6 R. W. Martin, P. R. Edwards, J. H. Rice, J. W. Robinson, A. Joujour, R. A. Taylor, R. Oliver and G. A. D. Briggs, *Phys. Status Solidi A*, 2005, **202**, 372.
7 J. H. Na, J. H. Rice, R. A. Taylor, R. Oliver and G. A. D. Briggs, *Appl. Phys. Lett.*, 2005, **86**, 083109.
8 M. Fanti, F. Zerbetto, J. P. Galaup, J. H. Rice, P. R. Birkett, N. Wachter and R. Taylor, *J. Chem. Phys.*, 2002, **116**, 7621.
9 S. Fraigne, J. H. Rice and J. P. Galaup, *J. Lumin.*, 2001, **94**, 649.
10 J. H. Na, J. H. Rice, R. A. Taylor, R. Oliver and G. A. D. Briggs, *Appl. Phys. Lett.*, 2005, **86**, 123102.
11 Z. Wang, C. J. Medforth and J. A. Shelnutt, *J. Am. Chem. Soc.*, 2004, **126**, 15954.
12 Q. Liu, J. Zhu, T. Sun, H. Zhou, Q. Shao, G. Li, X. Liu and Y. Yin, *RSC Adv.*, 2013, **3**, 2765.
13 N. T. H. White, G. S. Beddard, J. R. G. Thorne, T. M. Feehan, T. E. Keyes and P. Heathcote, *J. Phys. Chem.*, 1996, **100**, 12086.
14 G. D. Scholes, G. R. Fleming, A. Olaya-Castro and R. van Grondelle, *Nat. Chem.*, 2011, **3**, 763.
15 S. Sengupta and F. Würthner, *Chem. Commun.*, 2012, **48**, 5730.
16 K. Ariga, J. P. Hill, M. V. Lee, A. Vinu, R. Charvet and S. Acharya, *Sci. Technol. Adv. Mater.*, 2008, **9**, 014109.
17 S. Damm, N. C. Carville, B. J. Rodriguez, M. Manzo, K. Gallo and J. H. Rice, *J. Phys. Chem. C*, 2012, **116**, 26543.
18 N. C. Carville, M. Manzo, S. Damm, M. Castiella, L. Collins, D. Denning, S. A. L. Weber, K. Gallo, J. H. Rice and B. J. Rodriguez, *ACS Nano*, 2012, **6**, 7373.
19 Y. Yamamoto, T. Fukushima, Y. Suna, N. Ishii, A. Saeki, S. Seki, S. Tagawa, M. Taniguchi, T. Kawai and T. Aida, *Science*, 2006, **314**, 1761.
20 C. Röger, M. G. Müller, M. Lysetska, Y. Miloslavina, A. R. Holzwarth and F. Würthner, *J. Am. Chem. Soc.*, 2006, **128**, 6542.
21 C. J. Medforth, Z. Wang, K. E. Martin, Y. Song, J. L. Jacobsen and J. A. Shelnutt, *Chem. Commun.*, 2009, 7261.
22 Z. Wang, C. Medforth and A. Shelnutt, *J. Am. Chem. Soc.*, 2004, **126**, 15954–15955.
23 Q. Liu, J. Zhu, T. Sun, H. Zhou, Q. Shao, G. Li, X. Liub and Y. Yin, *RSC Adv.*, 2013, **3**, 2765.
24 Y. Qiu, P. Chen and M. Liu, *J. Am. Chem. Soc.*, 2010, **132**, 9644.
25 S. Okada and H. Segawa, *J. Am. Chem. Soc.*, 2003, **125**, 2792.
26 Y. Li, W. W. Han and M. Z. Liao, *Acta Phys.–Chim. Sin.*, 2009, **25**, 2493.
27 F. X. Wang, Y. Q. Liu, H. D. Wu, Y. Xiao and G. B. Pan, *J. Mater. Chem. C*, 2013, **1**, 422.
28 Z. Wang, L. E. Lybarger, W. Wang, C. J. Medforth, J. E. Miller and J. A. Shelnutt, *Nanotechnology*, 2008, **19**, 395604.
29 M. O. Senge, *Chem. Commun.*, 2006, 243.
30 Y. H. Zhang, Z. Y. Li, Y. Wu, Y. Z. Zhuc and J. Y. Zheng, *Spectrochim. Acta, Part A*, 2005, **62**, 83.
31 Y. H. Zhang, W. J. Ruan, Z. Y. Li, Y. Wu and J. Y. Zheng, *Chem. Phys.*, 2005, **315**, 201.
32 K. M. Barkigia, L. Chantranupong, K. M. Smith and J. Fajer, *J. Am. Chem. Soc.*, 1988, **110**, 7566.
33 S. A. MacGowan and M. O. Senge, *Chem. Commun.*, 2011, **47**, 11621.
34 M. O. Senge and W. W. Kalisch, *Inorg. Chem.*, 1997, **36**, 6103.
35 K. Hosomizu, M. Oodoi, T. Umeyama, Y. Matano, K. Yoshida, S. Isoda, M. Isosomppi, N. V. Tkachenko, H. Lemmetyinen and H. Imahori, *J. Phys. Chem. B*, 2008, **112**, 16517.
36 S. Hatscher and M. O. Senge, *Tetrahedron Lett.*, 2003, **44**, 157.
37 M. O. Senge, Y. M. Shaker, M. Pintea, C. Ryppa, S. S. Hatscher, A. Ryan and Y. Sergeeva, *Eur. J. Org. Chem.*, 2010, 237.
38 S. Gawinkowski, G. Orzanowska, K. Izdebska, M. O. Senge and J. Waluk, *Chem.–Eur. J.*, 2011, **17**, 10039.
39 Q. M. Tran, C. Fong, R. A. Rothery, E. Maklashina, G. Cecchini and J. H. Weiner, *PLoS One*, 2012, **7**, e32641.

40 S. E. J. Bell, J. H. Rice, J. J. McGarvey, R. E. Hester, J. N. Moore, R. N. Perutz, T. Q. Ye, Y. Mizutani and T. Kitagawa, *Laser Chem.*, 1999, **19**, 271.
41 R. F. Khairutdinov and N. Serpone, *J. Phys. Chem. B*, 1999, **103**, 761.
42 A. V. Udaltsov, L. A. Kazarin, V. A. Sinani and A. A. Sweshnikov, *J. Photochem. Photobiol., A*, 2002, **151**, 105.
43 S. Verma and H. N. Ghosh, *J. Phys. Chem. Lett.*, 2012, **3**, 1877.
44 D. L. Akins, H.-R. Zhu and C. Guo, *J. Phys. Chem.*, 1994, **98**, 3612.
45 J. H. Rice, *Mol. BioSyst.*, 2007, **3**, 781.
46 G. Hill, J. H. Rice, S. R. Meech, P. Kuo, K. Vodopyanov and M. Reading, *Opt. Lett.*, 2009, **34**, 431.
47 J. H. Rice, *Nanoscale*, 2010, **2**, 660.
48 Z. Chernia and D. Gill, *Langmuir*, 1999, **15**, 1625–1633.
49 A. Rosa, G. Ricciardi and E. J. Baerends, *J. Phys. Chem. A*, 2006, **110**, 5180–5190.
50 A. Stone and E. B. Fleischer, *J. Am. Chem. Soc.*, 1968, **90**, 2735–2748.
51 A. V. Udal'tsova, M. Tosakab and G. Kaupp, *J. Mol. Struct.*, 2003, **660**, 15–23.